CrossMark

Synthesis and Kinetics of Corrosion Inhibition of Water-Soluble Terpolymer of Polyvinyl Alcohol Functionalized with Vinyl Sulfonate and *p*-Vinyl Benzene Sulfonate, in Molar HCl

R. Geethanjali[1] · S. Subhashini[1]

Abstract

A water-soluble terpolymer polyvinyl alcohol-*g*-poly(vinyl sulfonate-*p*-vinyl benzene sulfonate) was synthesized by free radical polymerization of polyvinyl alcohol with monomers sodium salt of vinyl sulfonic acid and *p*-vinyl benzene sulfonic acid. The formation of terpolymer was confirmed using FTIR and ^{1}H NMR spectra and the thermal properties of the terpolymer were confirmed using TGA and DSC. The performance of the water-soluble terpolymer inhibitor for corrosion of mild steel in 1 M HCl solution at varying temperatures was investigated by weight loss, potentiodynamic polarization and electrochemical impedance spectroscopy. Weight loss measurements showed that the inhibitory character within the studied environment increased with increasing concentration, but highest efficiency was obtained with rise in temperature. Polarization results revealed that the terpolymer inhibitor functions as a mixed-type inhibitor providing an absolute control on both cathodic and anodic reactions. Impedance studies showed that the inhibitor's adsorption took place at the most active sites on the metal surface resulting in a homogenous surface. The inhibitive action of the terpolymer was explained in view of adsorption on the surface of steel. The surface coverage data were fitted to various adsorption isotherms and best-fit isotherm was selected for determination of thermodynamic parameters of adsorption. Supporting information pertaining to inhibitor adsorption on the metal surface was provided using surface imaging techniques like scanning electron microscopy and Atomic force microscope.

Keywords Terpolymer · Chemical adsorption · Mild steel · HCl · SEM · AFM

1 Introduction

The corrosion of mild steel is a perennial problem causing severe economic loss, material loss and structural damage to valuable instruments, etc., in industries that carry out acid pickling, industrial acid cleaning, acid descaling and oil well acidizing [1]. Several corrosion control methods have been developed to combat the corrosion including chrome treatment of steel surfaces, pickling inhibitors, sacrificial zinc layers, cathodic protection and anodic protection. The basic mechanism of corrosion inhibition involves (i) cathodic protection involving donation of charges or electrons from a sacrificial metal to the steel (ii) anodic protection involving withdrawing of charges or electrons from the steel and (iii) use of inhibitors involving formation of protective layer on the surface of the steel to separate it from the corrosive environment [2]. The use of inhibitors in pickling baths is one of the most practical approaches to protect mild steel from corrosive chloride ions.

Efforts are presently underway to develop cost effective and environmentally benign polymeric corrosion inhibitors. Polymers are found to be effective inhibitors, because of the superior properties compared to their monomer analogues. The long carbon chain linkages, functional groups and larger size of the polymer moieties aid themselves to anchor strongly on the metal surface. Moreover, the cost effectiveness of the polymer inhibitors is a practical advantage to be considered. The idea of polymerizing/blending/compositing stems from the fact of introducing multiple adsorption sites or inculcate special functional groups that render properties like solubility, degradability and processability. Recently,

✉ R. Geethanjali
  anjalirajj@gmail.com

1 Department of Chemistry, Avinashilingam Institute for Home Science and Higher Education for Women, Coimbatore, Tamil Nadu, India

some grafted polymers were reported as corrosion inhibitor like water-based acrylic terpolymer [3], PVA-based terpolymer [4–6], PVA-grafted amino acid [7–9] and so on [10–15]. This paper focuses on the use of water-soluble polymers as corrosion inhibitors for MS in hydrochloric acid medium. The water-soluble polymer used for the present work is a grafted terpolymer having polyvinyl alcohol (PVA) backbone grafted with poly(vinyl sulfonate-co-*p*-vinyl benzene sulfonate) polymer. The terpolymer PVA-VSA-PVBS is tailored such that it accommodates the necessary hetero atoms like S and O and an aromatic ring. Hence, the terpolymer of the present study can be claimed more advantageous as it is novel, water-soluble and has the necessary hetero atoms/anchoring moieties for adsorption on the metal surface.

2 Experimental Details

2.1 Inhibitors

The terpolymer PVA-VSA-PVBS was synthesized by free radical polymerization of the PVA and monomers sodium salt of vinyl sulfonic acid and *p*-vinyl benzene sulfonic acid in distilled water. PVA (2.5 g; mol wt. 1,40,000), *p*-vinyl benzene sulfonic acid (1 g) and vinyl sulfonic acid sodium salt (1.5 g) were dissolved in 80 mL of water. The whole reaction mixture was purged with nitrogen gas for half-an-hour. 10 mL of sodium dodecyl sulfonate solution (0.03 g) was mixed into the reaction solution. Then, 0.273 g of potassium persulfate dissolved in 10 mL water was added as an oxidant initiator. The reaction was allowed to continue for 3 h. Then the reaction mixture was added to fivefold volume of acetone to precipitate the product. The product was dried under vacuum for 24 h and utilized for further studies.

Total yield = 90%.

2.2 Material Preparation

The present studies were conducted by shearing the commercially available mild steel (MS) strips into $5 \times 1\ cm \times 2\ mm$ for immersion studies, and were cut into $1\ cm^2$ coupons fixed to a brass rod for all electrochemical studies. The MS strips were found to have following composition: C-0.106%, Mn-0.196%, P-0.027%, Cr-0.022%, S-0.016%, Ni-0.012%, Si-0.006%, Mo-0.003% and remainder Fe. Analar grade hydrochloric acid (Merck) was used for preparation of corrosive medium.

2.3 Weight Loss and Electrochemical Studies

Weight loss studies were conducted by immersing the MS strips in triplicates in 100 mL of 1M HCl solution with and without various concentrations of the inhibitor (0.03–0.45 wt.%) at various temperatures (303–343 K) for ½ an hour. The strips were taken out and neutralized with $NaHCO_3$. The samples were cleaned to remove corrosion products, dried and reweighed. All the experiments were carried out based on ASTM G31 standard procedure.

Electrochemical measurement unit containing Potentiostat/Galvanostat (model Solartron 1280 B) connected to a personal computer with softwares: Corrware and Zplot were used for electrochemical experiments. A saturated calomel electrode (SCE) and a platinum electrode were used as reference and counter electrode, respectively. The working electrode was polished with different grades of emery paper, rinsed with distilled water, dried and then immediately inserted into the glass cell that contained 100 mL of electrolyte solution. The electrode was kept immersed for 15 min in 1M HCl before starting the measurement to attain steady state.

Polarization studies were carried out from anodic potential of − 0.1 V to cathodic potential of − 1 V with respect to the corrosion potential at a sweep rate of 0.1667 mV/s. The corrosion current densities (I_{corr}) were determined from the intersection point of cathodic and anodic Tafel lines.

Electrochemical impedance measurements were carried out using AC amplitude of 10 mV at frequency sweep from of 20 kHz to 0.1 Hz. The data were collected by using Z plot software and interpreted with Z view software. The Stern–Geary equation for kinetics is used to determine the best-fit value of ba, bc, E_{corr} and I_{corr}. All the experiments were conducted at 303–343 K at aerated atmosphere.

2.4 Surface Analysis

Mild steel strips were immersed in inhibited (0.45 wt.% inhibitor) and uninhibited solution for 6 h. Then, the specimens were cleaned with distilled water, dried and analysed by SEM and AFM instrument (A.P.E research, model A100, Italy).

3 Results and Discussion

3.1 Characterization

3.1.1 FTIR Analysis

A broader peak corresponding to OH group can be figured out for the grafted polymer in the range of 3000–3600 cm^{-1}, which is due to the –OH stretching vibrations of PVA and VSA. The vibrational bands observed at 2985 cm^{-1} may be assigned to alkyl –CH and/or aromatic –CH stretching vibrations in the grafted terpolymer. The C=O stretching of the unhydrolyzed acetate groups of PVA is present at 1697 cm^{-1} in the grafted terpolymer.

The absorptions around 1250 cm^{-1} and a broad peak positioned in the range of 1000–1071 cm^{-1} are attributable to the C–O stretching and C–O–C stretching of the acetyl groups of PVA, respectively. The C–O stretching vibrations of the polymer can be pointed at 1295 cm^{-1}. The –CH rocking vibrations of PVA at 839 cm^{-1} are absent in the polymer.
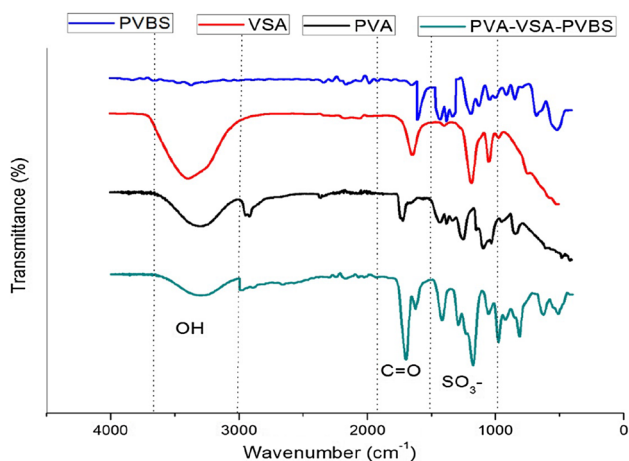
Fig. 1 Comparative FTIR spectrum of PVA-VSA-PVBS with its respective monomers

3.1.1.1 VSA Versus PVA-VSA-PVBS The peak at 2900–3700 cm^{-1} arises from the OH groups of SO$_3$H of the monomer. The antisymmetric and stretching modes of vibrations of SO$_3$ group can be observed at 1170 cm^{-1} and weak peak at 1054 cm^{-1}. The polymerization of the VSA monomer has been confirmed by the following peaks. This polymerized form of the monomer has been reported with a peak at 1195 cm^{-1} corresponding to the S=O group. The peak corresponding to the C=C str. in the monomer is absent in the polymer. The out-of-plane bending modes of the monomer vinyl unit of acrylamide and vinyl sulfonic acid positioned at 956 cm^{-1} disappear in the spectrum of the polymer.

3.1.1.2 PVBS Versus PVA-VSA-PVBS The absorption peaks at 1197, 1116 and 1046 cm^{-1} can be attributed to the asymmetric and symmetric stretching vibration of sulfonic acid group of the monomer. These peaks are the monomer slightly shifted and appear as a strong peak at 1170 cm^{-1} and weak peak at 1054 cm^{-1} in the grafted terpolymer (Figs. 1, 2). The out-of-plane bending vibrations of vinyl unit are observed at 983 and 919 cm^{-1} and the out-of-plane bending vibrations of the Ar–H bond of para-substituted benzene ring are observed at 839, 669 and 508 cm^{-1}. The grafted polymer has out-of-plane bending vibrations corresponding to Ar–H bond of substituted benzene ring at 974, 804, 643 and 481 cm^{-1} in the polymer.
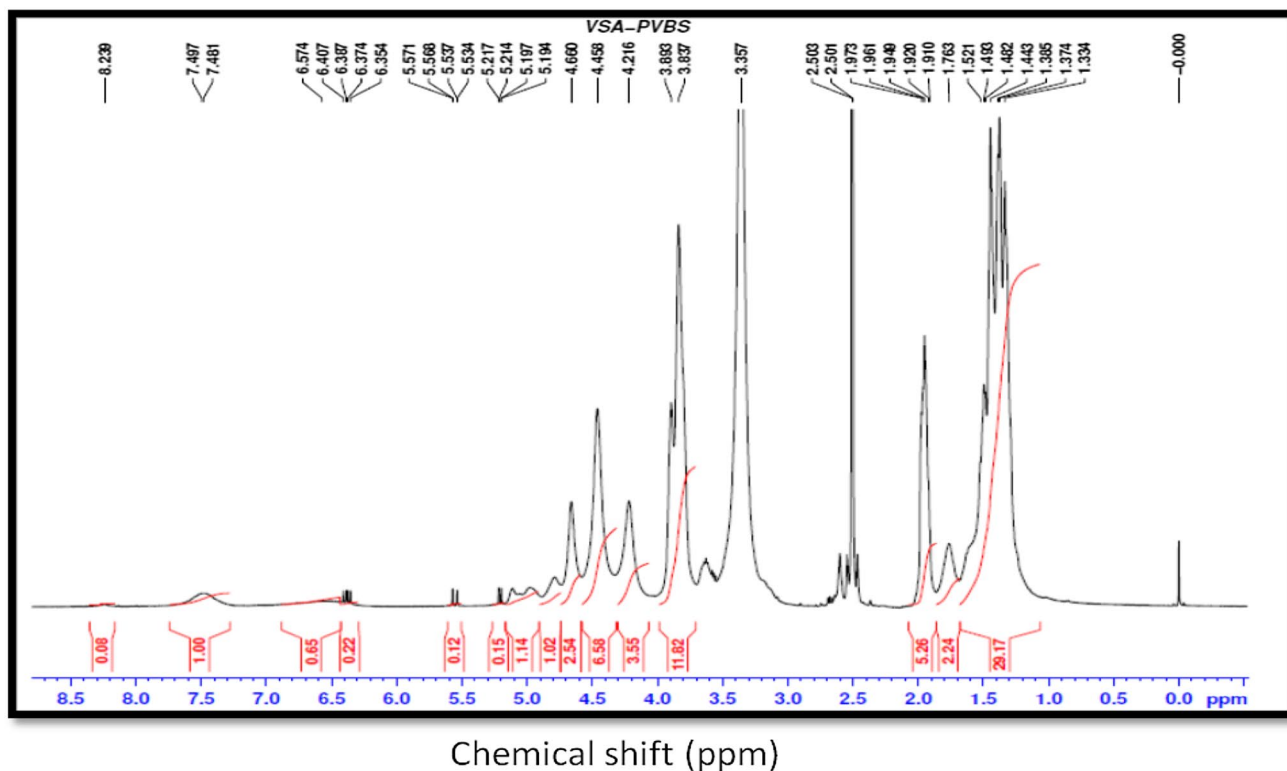
Fig. 2 Proton NMR spectrum of sample PVA-VSA-PVBS in DMSO-d6

3.1.2 Analysis of ^{1}H NMR Spectrum of PVA-VSA-PVBS

PVA-VSA-PVBS: *^{1}H NMR (500 MHz, DMSO-d6, δ ppm): 1.33–1.52(CH$_2$), 1.76, 1.91–1.97 (CH), 3.83–3.89(CH–OH), 4.67,4.47,4.23 (t,Ar–H), 7.49 and 6.35–6.57 (Ar–CH).*

The ^{1}H-NMR spectrum of the PVA-VSA-PVBS exhibits the strongest peaks, respectively, at 1.49 (CH$_2$–PVBS), 1.44 (CH$_2$–PVSA), 1.37 (CH$_2$–PVA) due to the three different methylene bridges in the terpolymer [16]. The second strongest peaks, respectively, at 1.97–1.91 ppm and 1.76 ppm could be because of the methine groups. The solvent peaks are manifested as sharp strong peaks at 2.5 ppm and 3.35 ppm. The broad peak centred at 3.89–3.83 ppm arises due to the –CH–OH of PVA [17]. The triplet positioned at 4.67, 4.47, 4.23 ppm is a manifestation of benzyl unit [18] of *p*-styrene sulfonic acid. The chemical shifts at 7.49 ppm (H$_a$) and 6.57–6.35 (q)(H$_b$) [19] are due to 2 different benzene protons. H$_b$ protons are split into a quartet initially by H$_a$ proton followed by long-range coupling with benzyl –CH$_2$ moiety of the polymer chain.

The IR spectral analysis and ^{1}H NMR analysis confirmed the terpolymer formation, and a tentative polymer structure is given in Fig. 3.

3.1.3 TGA Spectral Analysis of PVA-AA-VSA

Analysis of the TGA and DTG thermograms of PVA-VSA-PVBS (Fig. 4) shows that the degradations occur in three stages (Table 1). The first step with a weight loss of 8% can be due the loss of water molecules. The second degradation step is a peak at 263 °C with a small hump at 325 °C. In this range, 50% of the degradation has taken place that can be attributed to the desulfonation of the terpolymer. The final decomposition was found to occur at 422 °C resulting in 74% weight loss from the initial mass can be due to the breakdown of C–H bonds, decompositions of any intermediate
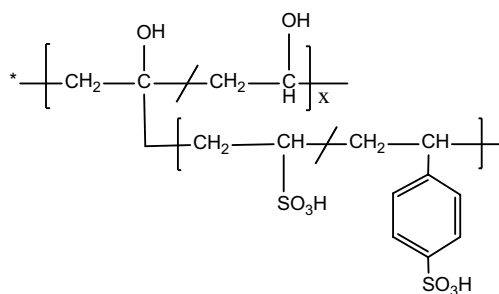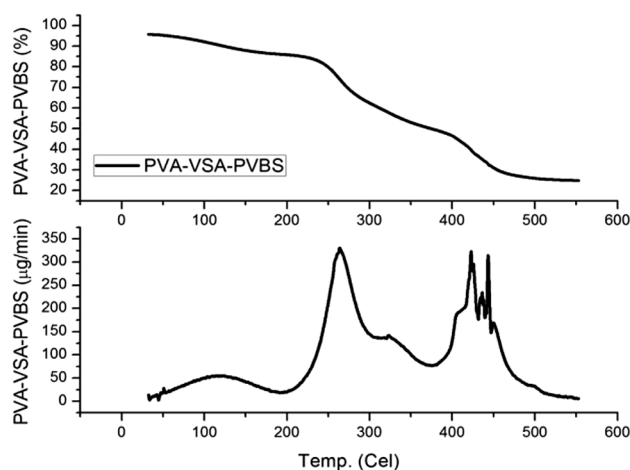

Fig. 4 TGA and DTG curves of PVA-VSA-PVBS

macromolecular product and degradation of aromatic fragments of styrene units.

3.1.4 DSC Analysis of PVA-VSA-PVBS

Figure 5 shows the calorimetric curve for the terpolymer PVA-VSA-PVBS with one broad peak. Glass transition is recorded as a very small step transition in the temperature range of 36–57 °C. The small Tg values associated with the polymer can be attributed to the high mobility of the polymeric segments in the domain [20].

The mobility of the polymeric segments is facilitated by the anionic repulsions that exist among the SO$_3^-$ groups. However, the melting endotherm is present as a broad peak. This widening of the transition when compared with the other polymers discussed above can be rationalized by the following arguments. The electrical charges associated with the anionic sulfonic acid groups of polyvinyl sulfonate and polyvinyl benzene sulfonic acid units are statistically distributed in the PVA domain thereby widening its chemical diversity and consequently the range of temperature leading to a broader peak. The onset melting point is recorded at 237 °C and the actual melting point is positioned at 332 °C. The enthalpy value recorded for the wide area is 491 mJ/mg.

The small difference in the Tg values can be partly attributed to the small difference in molecular weight and polydispersities of the compared polymers. The polymer–polymer interactions produce an amorphous phase that can induce a change in the crystalline structure of the polymer. Hence, the decrease in heat of fusion or increase in melting point represents the reduced perfection/crystallinity with increase in degree of cross-linking [21].

Fig. 3 Tentative structure of PVA-VSA-PVBS

Table 1 Weight loss % and its derivative obtained for PVA and PVA-VSA-PVBS during TG analysis

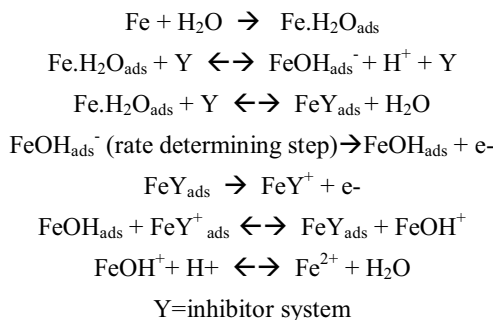| S. no.	Name of the polymer	TG wt. loss in %			DTG (°C)	
		100–200 °C	200–350 °C	350–450 °C	Td_i (°C)	Td_f (°C)
1	PVA	8	5	84	328	431
2	PVA-VSA-PVBS	5	55	84	282	422
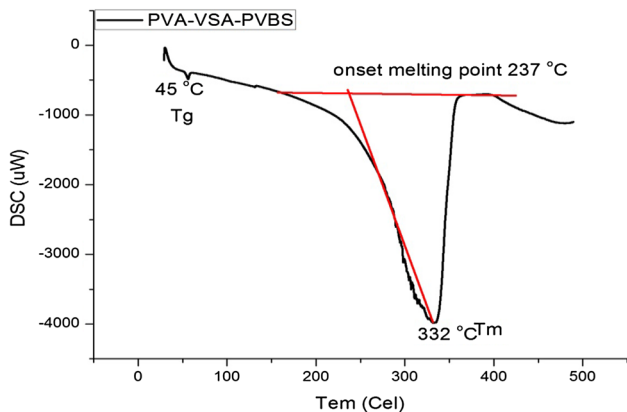
Fig. 5 DSC curve of terpolymer PVA-VSA-PVBS

3.2 Weight Loss Studies

3.2.1 Effect of Concentration

The effect of acid temperature in the range of 303–343 K in the presence and absence of the PVA-AA-VSA at various concentrations, and the deduced corrosion rates and IE are given in Table 2. The IE values of the terpolymers presented in Table 2 show a positive effect with respect to concentration. The terpolymers show an IE in the range of 65–70% for the low concentration, which increases to a maximum value around 80% for the highest concentration. This is an evidence for the adsorption of the polymers on the metal surface owing to multiple adsorption centres which makes the adsorption process favourable [22]. Amin et al. [22] explained this trend as increasing the inhibitor

concentration may lead to the formation of multilayers that could furnish a maximum IE beyond which what could be achieved by monolayers at low concentration. In other words, increase in concentration increases the adsorption and surface coverage of the inhibitor molecules; thus, the surface is efficiently separated from the medium.

Generally, adsorption of the inhibitors was found to occur by the exchange of water molecules adsorbed on the metal surface with inhibitor molecules. A detailed mechanism involving two adsorbed intermediate species in relation to the retardation of anodic dissolution of iron in the presence of inhibitor are as proposed by Ashassi-Sorkhabi and Nabavi-Amri [23].

$$Fe + H_2O \rightarrow Fe.H_2O_{ads}$$
$$Fe.H_2O_{ads} + Y \leftrightarrow FeOH_{ads}^- + H^+ + Y$$
$$Fe.H_2O_{ads} + Y \leftrightarrow FeY_{ads} + H_2O$$
$$FeOH_{ads}^- \text{ (rate determining step)} \rightarrow FeOH_{ads} + e-$$
$$FeY_{ads} \rightarrow FeY^+ + e-$$
$$FeOH_{ads} + FeY^+_{ads} \leftrightarrow FeY_{ads} + FeOH^+$$
$$FeOH^+ + H^+ \leftrightarrow Fe^{2+} + H_2O$$
$$Y = \text{inhibitor system}$$

Arukalam et al. [24] explained the above mechanism as follows: A corroding metal surface is non-homogenous due to the existence of lattice defects and dislocations, and are generally characterized by multiple adsorption centres. Inhibitor molecules having suitable adsorption enthalpies may thus be adsorbed more readily at the surface active

Table 2 Corrosion rates and IE obtained for various concentrations of PVA-VSA-PVBS at 303–343 K

Conc. wt.%	303 K		313 K		323 K		333 K		343 K	
	CR (mpy)	IE (%)	CR (mpy)	IE (%)	CR (mpy)	IE (%)	CR (mpy)	IE (%)	CR (mpy)	IE (%)
Blank	870.0		1825.3		5680.6		10713.1		18449.3	
0.03	366.8	57.8	742.1	59.3	2200.6	61.3	4597.4	57.1	6235.1	66.9
0.09	349.7	59.8	742.1	59.3	2055.6	63.8	3249.7	69.7	5356.5	71.6
0.18	332.7	61.8	690.9	62.1	1535.3	73.0	2499.1	76.7	5220.1	72.3
0.27	324.1	62.7	571.5	68.7	1228.2	78.4	2396.8	77.6	4529.2	76.0
0.36	315.6	63.7	571.5	68.7	1083.2	80.9	2004.4	81.3	4213.6	77.6
0.45	290.0	66.7	503.2	72.4	887.1	**84.4**	1987.4	81.4	4051.5	78.5

Highest efficiency value is given in bold

sites, i.e. when the formation of FeY_{ads} becomes energetically more favourable, the amount of $\overline{FeOH}_{ads}$ responsible for the rate determining step is lowered thus suppressing the anodic dissolution of iron. The inhibition efficiency discussed so far is achieved by blocking cathodic or anodic reaction through adsorption, but Amin et al. [22] explains that it can also be achieved by simply preventing the supply of oxidant or transport of reaction products. The latter occurs when the surface of the metal is saturated with monomolecular layers of the inhibitor, formation of multilayer layer occurs in which the inhibitor molecules are not in direct contact with the reactive sites of metal but offering additional resistance to transport of necessary elements for corrosion reaction. Hence, the increase in inhibition

Fig. 6 Effect of temperature on potentiodynamic polarization behaviour of MS in 1M HCl + PVA-VSA-PVBS

efficiency with concentration is related to adsorption and formation of a barrier film on the electrode surface.

3.2.2 Effect of Immersion Temperature

The effect of temperature on the inhibited acid-metal reaction is very complex because of certain changes that occur: Rapid etching, desorption of the inhibitor film and decomposition of inhibitor at higher temperature [25]. Observation of Table 2 shows that the corrosion rate was found to increase in the presence and absence of the inhibitor at various temperatures. The increase in corrosion rate was found to be more pronounced with increase in temperature for blank HCl solution. However, after the addition of inhibitors, the increase in corrosion rate with rise in temperature was less pronounced. This ensures the protective ability of the polymer. In the present systems studied, the IE gradually increased in the temperature domain range of 303–323 K (66.7–84.4% for 0.45 wt.% of inhibitor) and then decreased to 81.4% at 333 K and 78.5 at 343 K i.e. the protective nature of the film is interfered at 343 K rendering a less protective film which in turn allows the corrodant species to diffuse into the active sites initiating the corrosion [24]. Because increase in temperature stimulates kinetic energy of the metal surface which adversely affects the adsorption process. Hence, the adsorption–desorption equilibrium is shifted more towards the desorption process [26] and the electrode surface is more roughened owing to the enhanced corrosion.
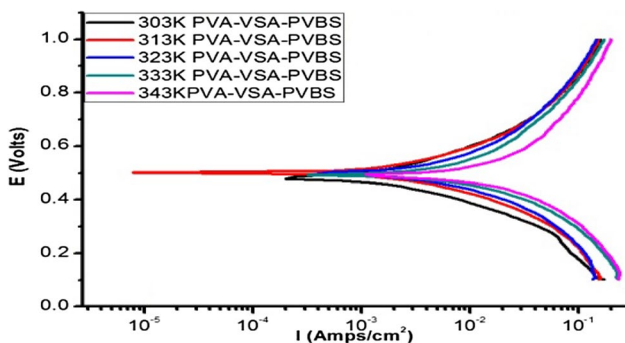
Table 3 Polarization parameters of the MS in 1 M HCl containing various concentrations of PVA-VSA-PVBS at 303–343 K calculated from extrapolation of the Tafel lines

T	Conc. wt.%	b_a (V)	b_c (V)	I_o (A/cm^2)	IE I_o (%)	R_p Ωcm^2	E_o (Volts)
303 K	Blank	0.220	0.269	0.01526		16.28	−0.4842
	0.09	0.147	0.185	0.00306	79.96	90.31	−0.4975
	0.27	0.153	0.183	0.00233	84.76	124.99	−0.5019
	0.45	0.151	0.183	0.00230	**84.93**	173.80	−0.5010
313 K	Blank	0.165	0.175	0.03723		7.80	−0.4805
	0.09	0.260	0.341	0.00669	82.03	35.24	−0.4960
	0.27	0.177	0.219	0.00381	89.78	48.25	−0.5001
	0.45	0.169	0.198	0.00354	**90.51**	80.00	−0.5012
323 K	Blank	0.167	0.202	0.06588		3.34	−0.4671
	0.09	0.348	0.446	0.01897	71.20	9.84	−0.4905
	0.27	0.221	0.297	0.01027	84.41	14.25	−0.4952
	0.45	0.223	0.296	0.00759	**88.49**	18.80	−0.4982
333 K	Blank	0.210	0.287	0.1204		2.63	−0.4840
	0.09	0.422	0.586	0.0338	71.90	5.26	−0.4401
	0.27	0.283	0.417	0.0241	79.98	8.34	−0.4876
	0.45	0.264	0.417	0.0183	**84.77**	12.87	−0.4930
343 K	Blank	0.230	0.431	0.3174		1.38	−0.4853
	0.09	0.979	2.368	0.0692	78.21	4.26	−0.4777
	0.27	0.404	0.544	0.0532	83.24	5.03	−0.4783
	0.45	0.419	0.724	0.0400	**87.41**	5.36	−0.4910

Highest efficiency values are given in bold

3.3 Effect of Temperature on Polarization Behaviour of PVA-VSA-PVBS

Both the anodic and cathodic polarization curves obtained for MS in 1M HCl solution in the presence and absence of optimum concentration of PVA-VSA-PVBS inhibitor at various temperatures are shown in Fig. 6. The corresponding electrochemical parameters such as corrosion potential (E_{corr}), Corrosion current (I_{corr}) and Inhibitor efficiency IE_{Icorr} derived are given in Table 3. When both the cathodic and anodic regions of the Tafel curves are observed, the current density decreases with the addition of inhibitor. Observation of Fig. 6 reveals that with progressive addition of the inhibitor (0.03–0.45 wt.%), the Tafel curves are shifted gradually to lower current densities. This shows that the inhibitor gets adsorbed on the metal surface thereby preventing the acid attack on the metal. The parallel nature of the current–potential curves indicates that hydrogen evolution reaction is activation controlled [27, 28]. The linearity of the Tafel lines is maintained with different slope values at all concentrations studied. This indicates that the adsorption of the inhibitors in the electrical double layer does not affect the mechanism of the process.

b_a and b_c values are affected by concentration of the inhibitors [29] indicating the inhibiting effect. The displacement in the E_{corr} values is less than 85 mV at 303 K which is an indication of mixed-type inhibitory action of the inhibitors. A notable decrease in the corrosion current density and increase in the polarization resistance was observed at all the temperature domains studied. This indicates that the addition of inhibitor reduces the corrosion current values even at high temperatures. Increase in R_p at higher temperatures is an indication of better inhibition of the interface against reactions associated with metal dissolution. Analysis of data from Table 3 reveals the positive influence of temperature on IE (IE_{Icorr}) till 323 K and then IE decreased. This shows that the terpolymer afforded a better and stable adsorbed film till 323 K which is well in accordance with static immersion studies. The decrease in IE is due to the disturbed stability of the adsorbed film on the metal surface due to the induced polarization combined with high temperature.

3.4 Effect of Temperature on Impedance Behaviour of PVA-VSA-PVBS

The effects of the PVA-VSA-PVBS concentration at 303–343 K on impedance behaviour of MS in HCl have been studied. Nyquist plot and representative Bode diagram for MS in HCl in the presence of various concentrations of PVA-VSA-PVBS are shown in Fig. 7a–c. Table 4 represents the list of electrochemical parameters obtained by fitting the data in a Randle's circuit (inset) as shown in Fig. 7.

Nyquist plot depicts a set of depressed capacitive loops generated for MS in blank HCl and inhibitor-added HCl. This depression at the high frequency region is a characteristic electrochemical corrosion reaction [30]. The solid electrodes are usually affected by these inhomogeneities and the resultant effect is termed as frequency dispersion effect [31, 32]. All the semicircles are single capacitive loop and similar in shape suggesting the geometric blocking effect of the inhibitor [33]. These similar shapes of the semicircles can also be attributed to the unmodified mechanism of the corrosion process before and after the addition of inhibitor. The addition of inhibitor poses no changes in the shape of the impedance indicating the activation-controlled nature of the reaction during charge transfer process [30]. But the effect of addition of the inhibitor is reflected as increase in diameter of the semicircle which takes place constantly at each level of inhibitor addition. The increase in diameter of the impedance at increasing concentration of the inhibitor augments the charge transfer resistance as well as the inhibition effect of the polymer [32].

Analysis of Table 4 shows that with increase in temperature in the presence of inhibitors

i. R_{ct} value decreases, C_{dl} increases (ii) the adsorption/desorption equilibrium is most probably shifted towards desorption. But at highest concentration of the inhibitor, the inhibiting adsorption layer is sustained. It may be due to the decrease in thickness of the adsorbed particles within outer Helmholtz layer (OHL) while the diffused portion of electrical double layer increases [34].

ii. Inspection of a set of data corresponding to a polymer reveals that the decrease in values of the CPE's exponent, n, with the rise of temperature is an indication for the increase of electrode surface roughness. The increase of n values with temperature reflects that the electrode surface becomes more homogeneous as a result of adsorption of the polymeric inhibitors [35]. The values of n are lower in pure acid than in the presence of inhibitors. This can be explained from an energetic point of view, i.e. the inhibitor's adsorption takes place at the most active sites on the metal surface isolation resulting in a homogenous surface [34].

iii. The relative values of IE% deduced from R_{ct} values are also included in Table 4 and it shows about 90% IE at 303 K and in the consequent higher temperatures the IE decreased. The decrease in the IE cannot be a bigger trait because the IE at all the studied temperatures are around 80–85% which is well correlated with the optimum IE obtained in weight loss experiments. The difference in the trend is usually expected because of the difference in the corrosion measurement techniques adopted. Conventional weight loss technique is
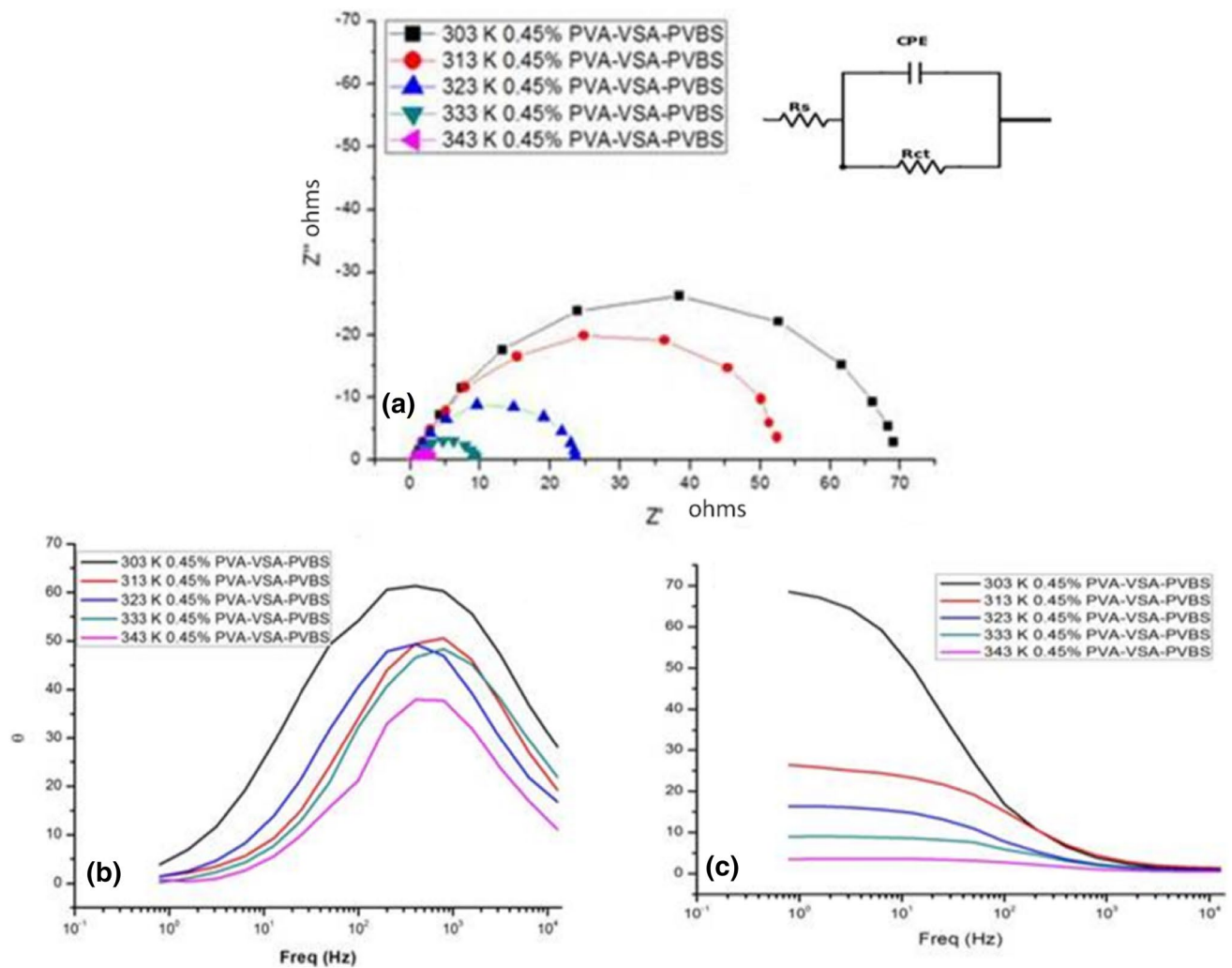
Fig. 7 **a** Nyquist, **b** phase angle plot, **c** bode plot for MS in 1 M HCl in the presence and absence of various concentrations of PVA-VSA PVBS fitted using the equivalent circuit (inset)

a natural process, whereas electrochemical techniques induce the corrosion rate instrumentally. However, in such cases, an overall perspective on the corrosion IE can be considered.

3.5 Adsorption Considerations

Adsorption of the inhibitor molecule on the metal surface can markedly change the corrosion-resisting ability of the metal. The surface coverage θ is calculated from the inhibition efficiency acquired from weight loss (IE_{WL}) and electrochemical studies (IE_{Icorr} and IE_{Rct}) and fitted into various isotherms: Langmuir, Temkin, El-Awady, Freundlich, Flory–Huggins, Frumkin and Bockris–Swinkles. Langmuir isotherm provided a higher regression values ($R^2 > 0.99$) but the slope values deviated from unity. This shows that the assumptions of Langmuir isotherm were ruled out and

hence other isotherm models were analysed .The data were found to provide a best fit in the Temkin isotherm model with regression values close to unity and the Temkin adsorption isotherm equation is represented as

$$\exp(-2a\theta) = KC, \tag{1}$$

where 'a' is called the molecular interaction parameter, which can be negative or positive, θ is the surface coverage, K is the adsorption equilibrium constant and C is the concentration of the inhibitor in wt.%. Positive values of 'a' relate to the attractive forces and negative values of 'a' relate to the repulsive forces that exist between adsorbed inhibitor molecules. When $-2a$ is represented as 'f' which describes the heterogeneity that prevails between the molecular interactions in the adsorption layer and the heterogeneity of the metal surface. Temkin equation can be represented in the transformed form as shown here.

Table 4 Impedance parameters of the MS in 1 M HCl containing various concentrations of PVA-VSA-PVBS at 303–343 K calculated from extrapolation of the Tafel lines

Temp.	Conc. wt.%	R_s Ω cm^2	Y_o*10^{-6}	n	R_{ct} kΩcm^2	IE_{Rct} (%)	$C_{dl}*10^3$ μF cm^{-2}
303 K	Blank	0.544	606.4	0.748	6.85		9.98
	0.09	0.605	308.5	0.803	40.47	83.07	3.13
	0.27	0.642	322.1	0.794	58.97	88.38	4.13
	0.45	0.671	327.0	0.789	70.09	**90.22**	4.82
313 K	Blank	0.771	546.7	0.749	4.14		7.29
	0.09	0.766	603.0	0.785	13.29	68.89	6.05
	0.27	0.811	623.7	0.788	15.82	73.86	5.37
	0.45	1.152	253.1	0.806	27.25	**84.83**	2.11
323 K	Blank	0.751	1236.1	0.684	2.26		48.10
	0.09	0.756	625.9	0.784	7.77	70.87	6.45
	0.27	0.738	595.5	0.790	10.55	78.54	6.13
	0.45	0.843	595.2	0.787	14.02	**83.85**	6.83
333 K	Blank	0.552	894.0	0.756	1.42		8.93
	0.09	0.685	706.3	0.776	3.40	58.21	6.69
	0.27	0.523	495.9	0.812	6.19	77.04	3.18
	0.45	0.490	617.1	0.791	8.00	**82.23**	5.82
343 K	Blank	0.729	883.2	0.723	0.69		10.04
	0.09	0.619	1141.9	0.798	2.19	68.35	8.30
	0.27	0.591	994.7	0.823	2.70	74.30	5.41
	0.45	0.486	1102.8	0.816	3.15	**77.97**	6.96

Highest efficiency values are given in bold

Table 5 Thermodynamic parameters of adsorption of PVA-VSA-PVBS on MS electrode surface in 1 M HCl solution (data from weight loss technique)

Temperature (K)	Statistical analysis		f	$K_{ads} \times 10^5$	ΔG_{ads} (kJmol-1)	ΔH_{ads} (kJmol-1)	ΔS_{ads} (Jmol-1 K^{-1})
	R^2	F					
303	0.90	46.88 (0.002)	34.75	1.41×10^{10}	− 69.00	− 122.2	− 216.9
313	0.80	62.93 (0.001)	19.73	2.38×10^6	− 48.67		
323	0.93	46.01 (0.002)	11.22	2.32×10^4	− 37.79		
333	0.99	49.92 (0.002)	11.29	2.34×10^4	− 38.97		
343	0.96	33.19 (0.005)	23.63	2.24×10^8	− 66.30		

$$\theta = \frac{1}{f} \ln K + \frac{1}{f} \ln C. \tag{2}$$

A plot of θ versus ln C (Fig. 7) gave straight lines with regression values almost equal to unity. The parameters including 'f' and 'K' were calculated from the slope and intercept, respectively, and are presented in Table 5. The validity of Temkin's isotherm is basically an evidence for the chemisorptive nature of adsorption. Since the obtained f values are greater than 0, it can be assumed that the adsorbed inhibitor molecules suffer repulsive forces among themselves [29, 30]. The free energy of adsorption ΔG_{ads} is calculated using the following relationship:

$$\log K_{ads} = -\log C_{H_2O} - \frac{\Delta G_{ads}}{RT}, \tag{3}$$

where C_{H_2O} is the molar concentration of water expressed in g/L, R is the molar gas constant J/mol/K and T is the temperature in K. The adsorption equilibrium constant K_{ads} is calculated from the intercept of straight line of Temkin isotherm. From the plot of ln K_{ads} versus 1/T, the adsorption enthalpy ΔH_{ads} and adsorption entropy ΔS_{ads} can be calculated from the slope and intercept, respectively, using the following equation.

$$\text{Ln } k_{ads} = -\frac{\Delta H_{ads}}{RT} + \frac{\Delta S_{ads}}{R}. \tag{4}$$

The values of f, K, ΔG_{ads}, ΔH_{ads} and ΔS_{ads} calculated using the Temkin relationship are listed in Table 5.

Analysis of Table 5 shows that the positive f values observed in all the systems describe the repulsive molecular interactions of adsorbed inhibitor molecules in the
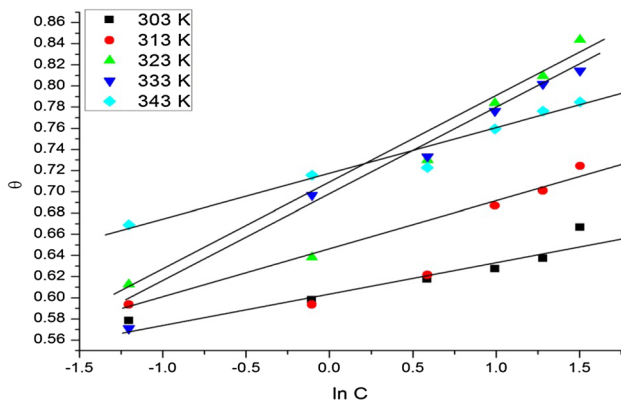
Fig. 8 Temkin isotherm of PVA-VSA-PVBS

adsorption layer (Fig. 8). The negative values of ΔG indicate the spontaneity of the adsorption process. Generally, the free energy values less than -20 kJ mol^{-1} are attributed to the electrostatic interaction between charged molecules and charged metal surface, and the phenomenon is termed as physisorption. The free energy values greater than -40 kJ mol^{-1} or more involve charge sharing or transfer from the inhibitor molecules to the metal surface to form a coordinate covalent bond, and the phenomenon is associated with chemisorption [36–38]. The values in the range of 21–39 kJ mol^{-1} can be attributed to the threshold for chemical adsorption in combination with physical adsorption [38, 39]. In the present investigation, the ΔG values are negative indicating the spontaneous adsorption process, and the magnitude is around 40 KJ mol^{-1}(-37 to 69 KJ mol^{-1}) which is consistent with the combined mode of adsorption as a result of sharing of electrons between the inhibitor molecule and metal surface to form a coordinate bond.

3.5.1 Enthalpy of Adsorption and Entropy of Adsorption

The sign of the ΔH can be used for distinguishing the adsorption of inhibitor as an exothermic process or endothermic process. The positive ΔH reflects the endothermic process and negative values of ΔH reflect the exothermic process. Endothermic process is generally attributed to chemisorption, but exothermic process can be associated with physisorption or chemisorption, depending on absolute values. A physisorption process reflects an enthalpy around 40 kJ mol^{-1} while chemisorption process results an enthalpy around 100 kJ mol^{-1} [38, 40]. The orderliness/disorderliness of an adsorption process can be determined using entropy of adsorption. The decrease in entropy or negative entropy is due to free movement of inhibitor molecules from the bulk solution that gets adsorbed in an orderly fashion onto the mild steel [41]. Similarly, the positive entropy is attributed to the solvent entropy that is

associated with the disorderliness of the solution during the adsorption process. The ΔH_{ads} obtained for the investigated polymer is -122 kJ mol^{-1}, which supports the chemical nature of adsorption through exothermic process. Hence, the adsorption of terpolymers can be concluded to have chemically adsorbed on the metal surface. Usually, negative enthalpy is associated with the decreased entropy.

The sign of entropy of adsorption is negative, meaning that the process of adsorption is accompanied by a decrease in entropy. This may be explained as follows: the chaotic degree at the metal/solution interface is higher before the adsorption of inhibitor molecules. But once when the inhibitor molecules start adsorbing on the metal solution interface, the orderliness of the adsorption is increased resulting in decreased entropy [41].

4 Surface Analysis

The application of adsorption isotherms provided a clear insight into the nature of adsorption. In order to analyse the external morphology (texture), crystalline structure, chemical composition, and orientation of materials, the present research work has taken advantage of the benefits offered by surface characterisation techniques: Scanning electron microscopy/energy dispersive X-ray analysis (SEM/EDX). Ex-situ corrosion product analysis was performed after 6-h immersion in the respective inhibited solution and uninhibited solution.

4.1 SEM Analysis of Metal Surface Inhibited with PVA-VSA-PVBS

Figure 9 shows the visual aspect of the mild steel surface after immersion in HCl containing PVA-VSA-PVBS. The surface morphology of the sulphur containing terpolymers deposited on mild steel clearly shows the distribution of spherical and non-spherical particles as well as some clusters. This may be interpreted as due to the adsorption of the inhibitor on the metal surface and forming a passive film in order to block the active site present on the mild steel surface. The elemental analysis results of the selected portion reveal the presence of O, Fe and S.

4.2 Surface Imaging Techniques-(ii) Atomic Force Microscopic Analysis

Atomic force microscope has emerged as a contemporary choice for investigating the influence of inhibitors on the metal surface from nanoscale to microscale level [42]. Because AFM uses a sharp tip to probe the surface features
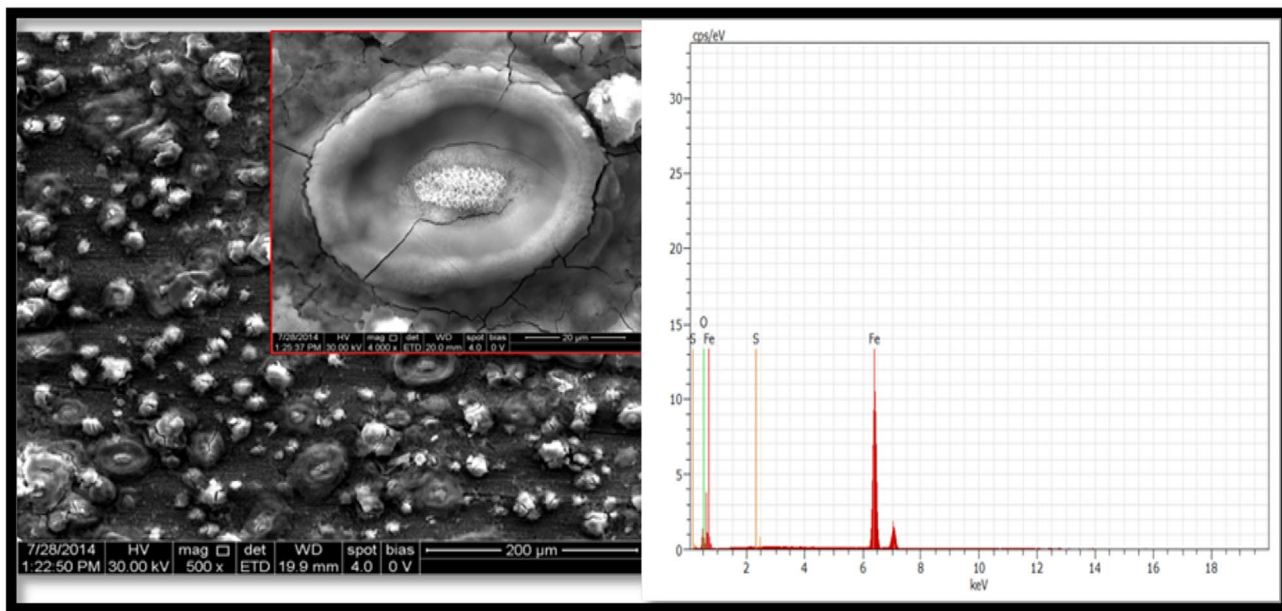
Fig. 9 SEM image and EDX spectra of mild steel in the presence of PVA-VSA-PVBS

Table 6 Surface roughness parameters obtained for MS under various conditions using atomic force microscope

Polished	Ra (µm)	Rms (µm)
Polished MS	0.112	0.146
Corroded	0.567	0.693
PVA-VSA-PVBS	0.329	0.404
Standard deviation	0.227	0.273

by raster scanning and can image the surface topography with extremely high magnifications, up to 1,000,000 X, comparable or even better than electronic microscopes. The measurements are depicted as three-dimensional images as horizontal $X–Y$ plane and the vertical Z plane. Resolution (magnification) at Z-direction is larger than $X–Y$. The integrity and persistence of inhibitor films formed on the metal surface is of paramount importance in the corrosion
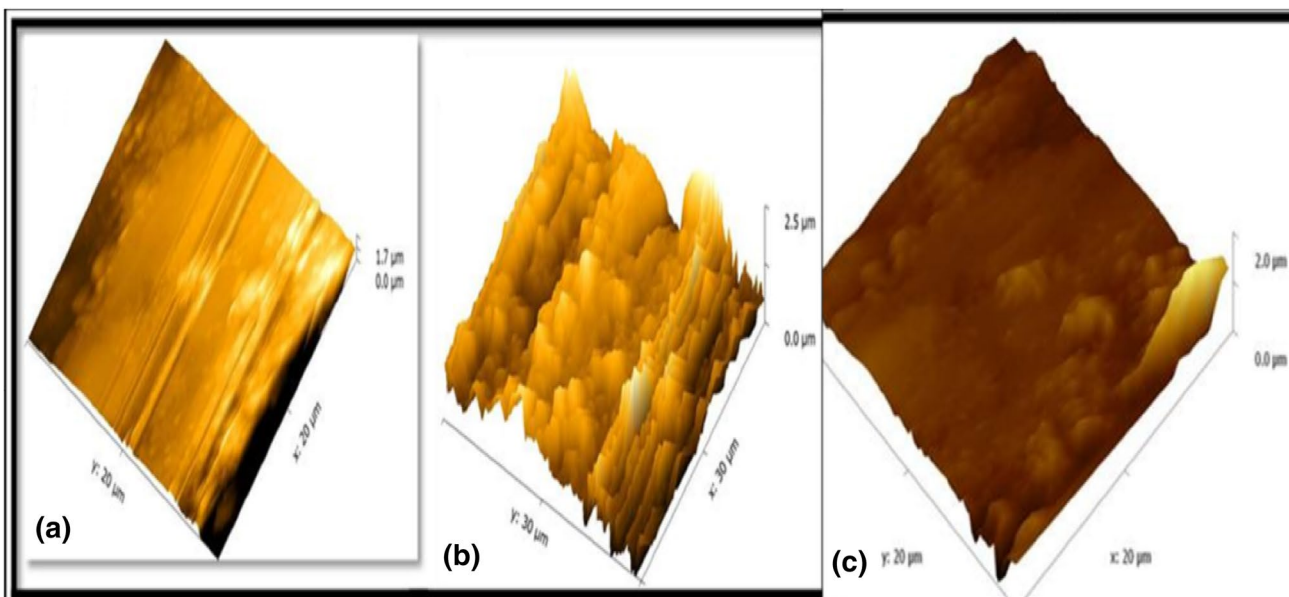

Fig. 10 AFM images of **a** polished MS, **b** corroded MS, **c** inhibited MS with PVA-VSA-PVBS

inhibition studies. The AFM technique reveals the extent of inhibitor film adsorption on the MS surface in terms of calculating the roughness parameter and through 3D images of the surface.

In the present study, morphological analyses of the surfaces of the mild steel were carried out by AFM in the range 0–50 μm at room temperature after immersion in different test solutions for 6 h. Three-dimensional AFM images of mild steel, mild steel immersed in 1 M HCl and mild steel immersed in 1 M HCl containing PVA-VSA-PVBS are shown in Fig. 10a–c, respectively. The roughness parameter Ra and root mean square roughness Rms were calculated using software called Gwyddion and are shown in Table 6.

The polished mild steel is absolutely smooth with very least surface roughness. In the absence of the inhibitors (Fig. 10b), the surface of the film shows several mountain-like formations that correspond to rough surface [43]. The Ra and Rms parameters corresponding to the MS corroded in blank HCl are 0.567 μm and 0.693 μm which are very higher than the roughness parameters obtained for inhibited surfaces. In the presence of inhibitors, the ridges caused by corrosive environment are decreased to a greater extent and a smooth surface is perceived. But still the surface resembles sand dunes which can be correlated to the uneven inhibitor film formed on MS surface during the course of the study.

5 Conclusion

The terpolymer PVA-VSA-PVBS was synthesized and a tentative structure of the polymer was proposed through the FTIR and NMR analysis. The thermal stability of the terpolymer was also discussed using Thermogravimetry and Differential scanning calorimetry. It was found that the efficiency of corrosion protection by adsorbed layers of PVA-VSA-PVBS strongly depends both on the concentration of the inhibitor and temperature, affording an IE between 80 and 85%. In polarization studies, PVA-VSA-PVBS acted as a mixed-type inhibitor in 1M HCl, and the inhibition was attributed to geometric blocking effect. EIS spectra exhibited one capacitive loop which shows that corrosion reactions were controlled by charge transfer phenomena. This was well established with the fact that inhibitor increased the R_{ct} values while decreased the C_{dl} values. The experimentally obtained results follow Temkin adsorption isotherm. Simultaneously, the surface coverage of the inhibitor on the mild steel was visually proved through images obtained from SEM ad AFM.

Compliance with Ethical Standards

Conflict of interest On behalf of all authors, the corresponding author states that there is no conflict of interest.

References

1. Abboud Y, Abourriche A, Saffaj T, Berrada M, Charrouf M, Bennamara A, Hannache H (2009) A novel azo dye, 8-quinolinol-5-azoantipyrine as corrosion inhibitor for mild steel in acidic media. Desalination 237:175–189

2. Fahlman M, Jasty S, Epstein AJ (1997) Corrosion protection of iron/steel by emeraldine base polyaniline: an X-ray photoelectron spectroscopy study. Synth Metals 85(1–3):1323–1326

3. Geethanjali R, Subhashini S (2016) Synthesis of water-soluble acryl terpolymers and their anticorrosion properties on mild steel in 1 mol L^{-1} HCl. CJCHE 24(4):543–552

4. Geethanjali R, Subhashini S (2014) Synthesis of water soluble Polyvinyl alcohol-based terpolymer and evaluation of corrosion inhibition property on mild steel in hydrochloric acid. Res J Recent Sci 3:170–176

5. Geethanjali R, Subhashini S (2016) Functionalization of PVA to synthesize *p*-vinyl benzene sulfonate terpolymers—A comparative study of anticorrosion, adsorption and activation. RSC Adv 6:100748–100758

6. Geethanjali R, Subhashini S (2015)). Thermodynamic characterization of metal dissolution and adsorption of polyvinyl alcohol-grafted poly (Acrylamide- Vinyl Sulfonate) on mild steel in hydrochloric acid. Portugaliae Electrochimica Acta 33(1):35–48

7. Subhashini S, Sabirneeza AAF (2011) Gravimetric and electrochemical investigation of water soluble poly (Vinyl Alcohol-Threonine) as corrosion inhibitor for mild steel. Proceedings of the World Congress on Engineering and Computer Science 2011 2011, II, pp. 19–21

8. Sabirneeza AAF, Subhashini S, Rajalakshmi R (2013) Water soluble conducting polymer composite of polyvinyl alcohol and leucine: an effective acid corrosion inhibitor for mild steel. Mater Corros 64(1):74–82

9. Sabirneeza AAF, Geethanjali R, Subhashini S (2014) Polymeric corrosion inhibitors for ferrous and its alloys—A review. *Chem Eng Commun*, https://doi.org/10.1080/00986445.2014.934448

10. Mansri A, Bouras B, Hammouti B, Warad I, Chetouani A (2013) Synergistic effect of AM-4VP-9 copolymer and iodide ion on corrosion inhibition of mild steel in 1 M H$_2$SO$_4$. Res Chem Intermed 39:1753–1770

11. Nwanonenyi SC, Obasi HC, Oguzie EE (2017) Inhibition and adsorption of polyvinyl acetate (PVAc) on the corrosion of aluminium in sulphuric and hydrochloric acid environment. J Bio Tribo Corros 3:53. https://doi.org/10.1007/s40735-017-0114-z

12. Rashid M, Waware US, Rahim AA, Hamouda AM (2018) *N*-cetyl-*N,N,N* trimethyl ammonium bromide (CTAB)-stabilized polyaniline: a corrosion inhibitor for mild steel. Anti-Corros Methods Mater 65(2):146–151

13. Jmiaia A, El Ibrahimia B, Tarab A, El Issamia S, barab OJ, Bazzia L (2018) Alginate biopolymer as green corrosion inhibitor for copper in 1M hydrochloric acid: experimental and theoretical approaches. J Mol Struct 1157:408–417

14. Srivastava V, Chauhan DS, Joshi PG, Maruthapandian V, Sorour AA, Quraishi MA (2018) PEG-functionalized chitosan: a biological macromolecule as a novel corrosion inhibitor, *Chem Select*.3, 7, 1990–1998

15. Quadri TW, Olasunkanmi LO, Fayemi OE et al (2017) Zinc oxide nanocomposites of selected polymers: synthesis,

characterization, and corrosion inhibition studies on mild steel in HCl solution. ACS Omega 2:8421–8437

16. Fernández MD, Fernández MJ, Hoces P (2008) Poly(vinyl acetal)s containing electron-donor groups: synthesis in homogeneous phase and their thermal properties. React Func Polym 68(1):39–56

17. Hiran B, Paliwal SN (2008) Synthesis and free radical copolymerization of N- [4-N-(Benzyl amino- carbonyl) phenyl] maleimide with methyl methacrylate. Malays Polym J 3(2):1–12

18. Yang JC, Jablonsky MJ, Mays JW (2002) NMR and FT-IR studies of sulfonated styrene-based homopolymers and copolymers. Polymer 43:5125–5132

19. Baradie B, Shoichet SM (2005) Novel fluoro-terpolymers for coatings applications. Macromolecules 38:5560–5568

20. Guirguis OW, Moselhey MTH (2012) Thermal and structural studies of poly(vinyl alcohol) and hydroxypropyl cellulose blends. Nat Sci 4(1):57–67

21. Ali SA, Saeed MT, El-sharif AMZ (2012) Diallyl-1,12-diaminododecane-based cyclopolymers and their use as inhibitors for mild steel corrosion. Polym Eng Sci 52(12):2588–2596

22. Amin M, El-rehim A, El-sherbini SS, Hazzazi EEF, O. A. and Abbas MN (2009) Polyacrylic acid as a corrosion inhibitor for aluminium in weakly alkaline solutions. Part I: weight loss, polarization, impedance EFM and EDX studies. Corros Sci 51(3):658–667

23. Ashassi-Sorkhabi H, Nabavi-Amri SA (2000), Corrosion inhibition of carbon steel in petroleum /water mixtures by n-containing compounds, *Acta Chimica Slovenica*,47, 507–517

24. Arukalam IO, Madufor IC, Ogbobe O, Oguzie E (2014) Experimental and theoretical studies of hydroxyethyl cellulose as inhibitor for acid corrosion inhibition of mild steel and aluminium. Open Corros J 6:1–10

25. Belkaid S, Tebbji K, Mansri A, Chetouani A, Hammouti B (2012) Poly(4-vinylpyridine-hexadecyl bromide) as corrosion inhibitor for mild steel in acid chloride solution. Res Chem Intermed 38(9):2309–2325

26. Fares MM, Maayta AK, Al-qudah MM (2012) Pectin as promising green corrosion inhibitor of aluminum in hydrochloric acid solution. Corros Sci 60:112–117

27. Tebbji K, Faska N, Tounsi A, Oudda H, Benkaddour M, Hammouti B (2007) The effect of some lactones as inhibitors for the corrosion of mild steel in 1 M hydrochloric acid. Mater Chem Phys 106:260–267

28. Atta A, Elsockary M, Kandil O, Shaker N (2008) Nonionic surfactants from recycled poly(ethylene terephthalate) as corrosion inhibitors of steel in 1 M HCl. J Dispers Sci Technol 29(1):27–39

29. Popova A, Christov M, Zwetanova A (2007) Effect of the molecular structure on the inhibitor properties of azoles on mild steel corrosion in 1M hydrochloric acid. Corros Sci 49(5):2131–2143

30. Torres VV, Rayol VA, Magalhães M, Viana GM, Aguiar LCS, Machado SP, Elia ED (2014) Study of thioureas derivatives synthesized from a green route as corrosion inhibitors for mild steel in HCl solution. Corros Sci 79:108–118

31. Ghailane T, Balkhmima RA, Ghailane R, Souizi A, Touir R, Touhami ME, Komiha N (2013) Experimental and theoretical studies for mild steel corrosion inhibition in 1 M HCl by two new benzothiazine derivatives. Corros Sci 76:317–324

32. Chen W, Luo HQ, Li NB (2011) Inhibition effects of 2,5-dimercapto-1,3,4-thiadiazole on the corrosion of mild steel in sulphuric acid solution. Corros Sci 53(10):3356–3365

33. Bentrah H, Rahali Y, Chala A (2014) Gum Arabic as an eco-friendly inhibitor for API 5L X42 pipeline steel in HCl medium. Corros Sci 82:426–431

34. Popova A, Sokolova E, Raicheva S, Christov M (2003) AC and DC study of the temperature effect on mild steel corrosion in acid media in the presence of benzimidazole derivatives. Corros Sci 45(1):33–58

35. Morad MS, El-Dean AMK (2006) 2,2′-Dithiobis(3-cyano-4,6-dimethylpyridine): a new class of acid corrosion inhibitors for mild steel. Corros Sci 48(11):3398–3412

36. Ahamad I, Quraishi MA (2009) Bis (benzimidazol-2-yl) disulphide: an efficient water soluble inhibitor for corrosion of mild steel in acid media. Corros Sci 51(9):2006–2013

37. Obot IB, Obi-Egbedi NO (2008) Fluconazole as an inhibitor for aluminium corrosion in 0.1M HCl. Colloids Surf A 330(2–3):207–212

38. Noor E, Al-Moubaraki AH (2008) Thermodynamic study of metal corrosion and inhibitor adsorption processes in mild steel/1-methyl-4[4′(-X)-styryl pyridinium iodides/hydrochloric acid systems. Mater Chem Phys 110(1):145–154

39. Li X, Deng S, Fu H, Mu G (2008) Synergistic inhibition effect of rare earth cerium (IV) ion and anionic surfactant on the corrosion of cold rolled steel in H$_2$SO$_4$ solution. Corros Sci 50:2635–2645

40. Awad MI (2006) Eco friendly corrosion inhibitors: inhibitive action of quinine for corrosion of low carbon steel in 1 M HCl. J Appl Electrochem 36(10):1163–1168

41. Li X, Deng S, Fu H (2010) Inhibition effect of methyl violet on the corrosion of cold rolled steel in 1.0M HCl solution. Corros Sci 52(10):3413–3420

42. Xianghong L, Guannan M (2005) Tween-40 as corrosion inhibitor for cold rolled steel in sulphuric acid: weight loss study, electrochemical characterization, and AFM. Appl Surf Sci 252:1254–1265

43. Quraishi MA, Shukla SK (2009) Poly (aniline-formaldehyde): a new and effective corrosion inhibitor for mild steel in hydrochloric acid. Mater Chem Phys 113:685–689